

Supplementary data

Fe(III) and Ni(II) Imidazole-Benzimidazole Mixed-Ligand Complexes: Synthesis, Structural Characterization, Molecular Docking, DFT Studies, and Evaluation of Antimicrobial and Anti-Inflammatory Activities

Nourah Almulhim¹, Hany M. Abd El-Lateef^{1*}, Mohamed Gouda¹, Mai M. Khalaf¹, Aly Abdou^{2*}

¹ Department of Chemistry, College of Science, King Faisal University, Al-Ahsa 31982, Saudi Arabia

² Department of Chemistry, Faculty of Science, Sohag University, Sohag 82524, Egypt

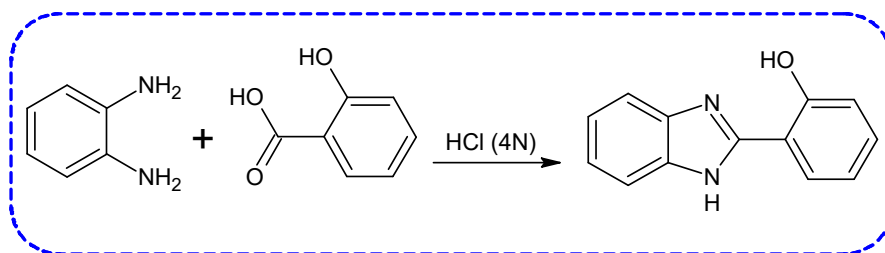
Corresponding authors: hmahmed@kfu.edu.sa (H. M. Abd El-Lateef.);

aly_abdou@science.sohag.edu.eg (A. Abdou)

2.2.2. Synthesis of the BZ ligand

2-(1H-benzimidazol-2-yl)phenol (BZ) co-ligand, was prepared as previously reported [1-3]: A mixture of o-phenylene-diamine (50.0 mmol, 5.4 g) and salicylic acid (50.0 mmol, 6.9 g) was refluxed for 8.0 h in presence of hydrochloric acid (4.0 N, 10.0 mL) on a water bath at 70 °C. Then, the reaction mixture was cooled and neutralized with potassium bicarbonate until the end of the effervescence. The obtained precipitate was collected by filtration and recrystallized from ethanol, Scheme (S.1).

BZ co-ligand: 2-(1H-benzimidazol-2-yl)phenol: Color: buff solid, yield: 60 %. ¹H-NMR, (DMSO-d₆) (δ, ppm): 15.40 (s, 1H, Ar-OH): 10.12 (s, 1H, -NH): 7.96-7.11 (m, 8H, Ar-H). FT-IR, (ν, cm⁻¹): Ar-OH (3311), -NH (3194), -C=N (1574). UV-vis. (λ_{max}, nm): 235 (π→π*) and 320 (n→π*).

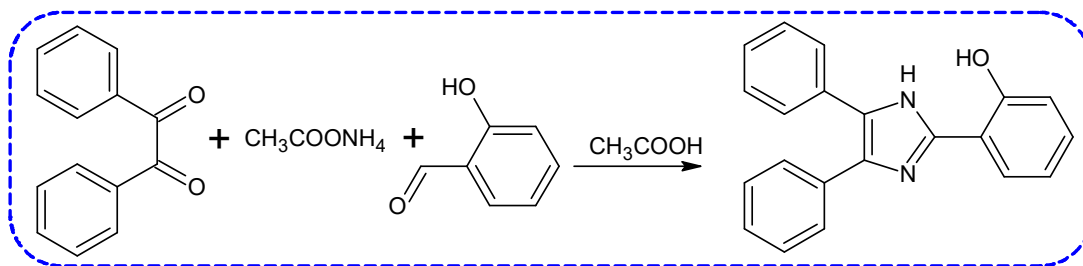


Scheme (S.1): synthesis of BZ ligand

2.2.3. Synthesis of the IM ligand

The 2-(4,5-diphenyl-1H-imidazol-2-yl)phenol (**IM**) co-ligand was prepared as previously reported [1-3]: a 100.0 mL single neck round bottomed flask was charged with a mixture of the 2-hydroxybenzaldehyde (10.0 mmol, 2.44 g), benzil (10.0 mmol, 1.22 g), and ammonium acetate (50.0 mmol, 3.85 g) in 10.0 mL of glacial acetic acid. A reflux condenser was set up and this solution was kept under reflux for 8 h. Afterwards, the mixture was poured to ice-cold de-ionized water, forcing the precipitation of the ligand: the crude product was collected by filtration, washed with ethanol, and finally re-crystallized from ethanol (Scheme 1). Detailed information is given in the Supporting Information Scheme (S.2).

IM ligand: 2-(4,5-diphenyl-1H-imidazol-2-yl)phenol: Color: Pale yellow solid, m.p. 210 °C, yield: 65 %. ¹H-NMR, (DMSO-d₆) (δ, ppm): 12.97, 12.93 (2H, -NH group and intramolecular hydrogen bond [-C=N.....H-O-]), 8.06-6.93 (m, 14H, Aromatic protons). FT-IR, (ν, cm⁻¹): C=N.....H-O- (3191, 3141), -C=N (1588). UV-vis. (λ_{max}, nm): 210 (π→π*) and 315 (n→π*).



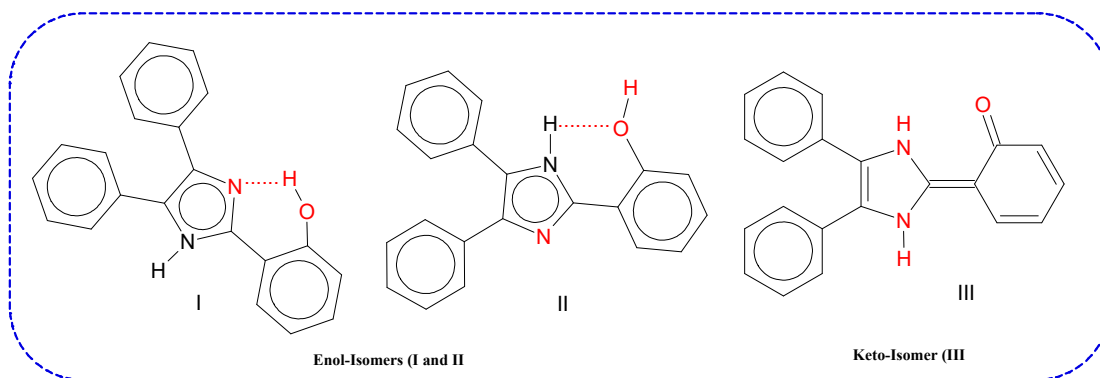
Scheme (S.2): synthesis of IM ligand

3.1.2. Structure elucidation of BZ ligand

The ^1H -NMR spectrum of BZ showed characteristic signal at 15.40 ppm (s, 1H) which was attributed to the Ar-OH. Moreover, the -NH proton, was observed at ≈ 10.12 ppm (s, 1H). While the aromatic protons had appeared at ≈ 7.96 -7.11 ppm (m, 8H), -, Fig. (S.1). FT-IR spectra showed characteristic band corresponding to Ar-OH group at $\approx 3303\text{ cm}^{-1}$. The -NH group appeared at 3200 cm^{-1} , Fig. (S.1). UV-Vis. spectra showed absorption bands at $\lambda_{\text{max}} \approx 235\text{ nm}$ ($\pi \rightarrow \pi^*$) and 320 nm ($n \rightarrow \pi^*$), Fig. (S.1).

3.1.3. Structure elucidation of IM ligand

The ^1H NMR spectrum, Fig. (S.2), showed -NH groups of the imidazole ring and phenolic -OH together at ca. 12.97, 12.53 ppm (2H), which confirm the presence of intramolecular hydrogen bonds ($-\text{C}=\text{N} \cdots \text{H}-\text{O}-$), as in the enol isomeric form (I) [4], Scheme (S.3). The aromatic protons appeared as multiplet signals in the range of 8.06–6.93 ppm (14H). Both, IR and ^1H NMR spectra confirmed the formation of IM ligand with the presence of intramolecular hydrogen bond. The quantum chemical calculations suggested that isomer I has higher stability than the other isomers (II and III). This revealed that only isomer I is stable under the experimental conditions [5]. The FT-IR spectra of the HI co-ligand, Fig. (S.2), exhibited characteristic bands at ca. 1588 cm^{-1} due to $-\text{C}=\text{N}$ of the imidazole ring. However, the appearance of two weak bands at 3191 and 3141 cm^{-1} proposed the presence of intramolecular hydrogen bonding [6] ($-\text{N} \cdots \text{H}-\text{O}-$), between the phenolic (-OH) and the imidazole nitrogen ($-\text{C}=\text{N}$), led to form either enol-isomers (I, II) or keto-isomer, (III) [7], Scheme (S.2). UV-Vis spectra of HI, Fig. (S.2), showed two absorption bands at 210 and 315 nm. The former is due to the $\pi \rightarrow \pi^*$ transition, whereas the later corresponds to the non-bonding electron pairs of the $-\text{C}=\text{N}$ chromophore.



Scheme (S.3): The enol-isomers (I: II) and keto-isomer (I) of **HII** ligand.

3.2. Characterization

The elemental analyses (C, H, and N) were performed using a Perkin-Elmer 2408 analyzer. The %M was determined using Atomic Absorption Spectroscopy (AAS) using Perkin- Elmer 2380 atomic absorption spectrometer. On a BRUKER FT-IR model 8101, IR spectra were measured. The Jasco V-750 UV-Vis spectrophotometer was used to detect UV-Vis spectra. Mass spectra were carried out using Direct Inlet part to the mass analyzer in Thermo Scientific GCMS model ISQ. The thermal degradation of the named compounds (TGA and DTA) was measured using a Shimaduz analyzer model 60 H at a heating rate of 10 °C min⁻¹. JENWAY conductivity meter model 4320 was used to measure molar conductance (of 10⁻³ mol/L DMF solution). The Bartington Susceptibility instrument model 4320 was used to test the molar magnetic susceptibility of powdered samples. The spectrophotometric contentious variation method [1] was used to calculate the stoichiometry of the metal complexes.

Stoichiometry of the synthesized mixed-ligand complexes

The continuous variation method was used to establish the composition of the ternary (M : IM: BZ) complexes [8, 9]. The molar fractions of two of the components were varied continuously, keeping their total concentration constant in the presence of a large excess of the third component. Under these conditions, the ternary system was modified to a pseudo-binary system [8, 9].

Firstly, for determination of the stoichiometry of M : IM in the presence of BZ as mixed ligands. A series of solutions containing different ratios of M: IM, were prepared (in the presence of an excess of BZ), keeping the total concentration of both M ion and IM constant. The ratio of M: IM, was determined from the relationship between absorbance (Abs) (at the λ_{\max} of the target complex) and mole fraction of IM ($IM / (IM + M)$).

Secondly, the ratio of M: BZ was determined as described above in the presence of excess (IM). A series of solutions containing different ratios of M: BZ, were prepared (in the presence of an excess of IM), keeping the total concentration of both M ion and BZ constant. The ratio of M: BZ, was determined from the relationship between absorbance (Abs) (at the λ_{\max} of the target complex) and mole fraction of BZ ($BZ / (BZ + M)$).

The results proved the 1:1:1 (M: IM: BZ.) ternary complexes were formed for FeBZIM, and NiBZIM complexes.

S.3. DFT calculations of reactivity descriptors

The optimized BZ, IM, and their corresponding FeBZIM and NiBZIM complexes were analyzed through optimization with the help of DFT/B3LYP combined with the 6-311G(d, p) basis set for C, H, N, O, and Cl atoms and [10-12] basis set for metal atoms. The reactivity descriptors, electron affinity (A), ionization potential (I), energy gap (ΔE), electronegativity (χ), electronic chemical potential (CP), chemical hardness (η), softness (σ), electrophilicity index (ω), and nucleophilicity (Nu), were computed based on equations (S.1-S.9).

$I = -E_{\text{HOMO}}$	equation (S.1)
$A = -E_{\text{LUMO}}$	equation (S.2)
$\Delta E = I - A$	equation (S.3)
$X = -(E_{\text{LUMO}} + E_{\text{HOMO}})/2$	equation (S.4)
$CP = (E_{\text{HOMO}} + E_{\text{LUMO}})/2$	equation (S.5)
$\eta = -(E_{\text{LUMO}} - E_{\text{HOMO}})/2$	equation (S.6)
$\sigma = 1/\eta$	equation (S.7)
$\omega = \mu^2/2\eta$	equation (S.8)
$Nu = 1/\omega$	equation (S.9)

Biological assay

***In Vitro* antimicrobial activity**

***In Vitro* Antibacterial activity**

The *in vitro* antibacterial activities of IM and BZ ligands, along with their FeBZIM and NiBZIM complexes were evaluated against two Gram-positive bacterial strains (*B. Subtilis*, and *S. Aureu*), and two Gram-negative bacteria strains (*E. coli*, and *k. pneumonia*) using the disk diffusion method [13]. A 100 μ L suspension of each bacterium, containing approximately 0.5×10^6 CFU, was evenly spread onto Muller Hinton Agar plates using a sterile swab. The compounds were dissolved in DMSO at a concentration of 1.5 mg/mL, and sterile discs (6 mm in diameter) were impregnated with the solutions and placed on the inoculated agar surface. The plates were inverted and incubated at 37 °C for 24 hours. As the samples diffused, bacterial growth was inhibited around the discs. After incubation, the antibacterial efficacy was assessed by measuring the diameter of the inhibition zones in millimeters. DMSO, serving as the solvent, showed no effect on bacterial growth and was used as a negative control.

***In Vitro* Aantifungal activity**

The antifungal activity screening was conducted using the disk diffusion method. The antifungal properties of the ligand and its complexes were tested against two fungal strains, *Candida albicans*, and *Aspergillusniger*. In this procedure, discs were soaked in compound solutions at a concentration of 1.5 mg/mL in DMSO and placed at various positions on Sabouraud Dextrose Agar plates inoculated with fungal spore suspensions (10^5 CFU/mL) [14]. The plates with *Candida albicans*, and *Aspergillusniger* were incubated at 32 °C for 24 hours and 37 °C for 7 days, respectively. Following incubation, the inhibition zones (measured in millimeters) formed around each disc was recorded to assess the antifungal activity of the compounds.

Activity Index (%)

The effectiveness of the antibiotic amoxicillin and the antifungal agent clotrimazole was also evaluated using the same methods to determine their efficacy as standard antibacterial and antifungal agents against the tested microorganisms. The % Activity Index was calculated by dividing the inhibition zone (IZ) of the test compound by the IZ of the standard drug and multiplying by 100 [15]. This comparison provided a comprehensive assessment of the antibacterial and antifungal activities of the compounds in relation to the standard drugs, amoxicillin and clotrimazole.

Minimum inhibitory concentration (MIC)

The Minimum Inhibitory Concentrations (MICs) were determined using the broth dilution method. In this procedure, each sample was dissolved in DMSO at various concentrations ranging from 10.0 to 200 μM under sterile conditions. To each tube containing the sample, 650 μL of Muller Hinton Broth and 100 μL of the tested microorganism were added. The tubes were then incubated at 37 °C for 24 hours. The MIC was defined as the lowest concentration of the antibacterial sample that inhibited visible microbial growth, as indicated by the absence of turbidity in the mixture [16].

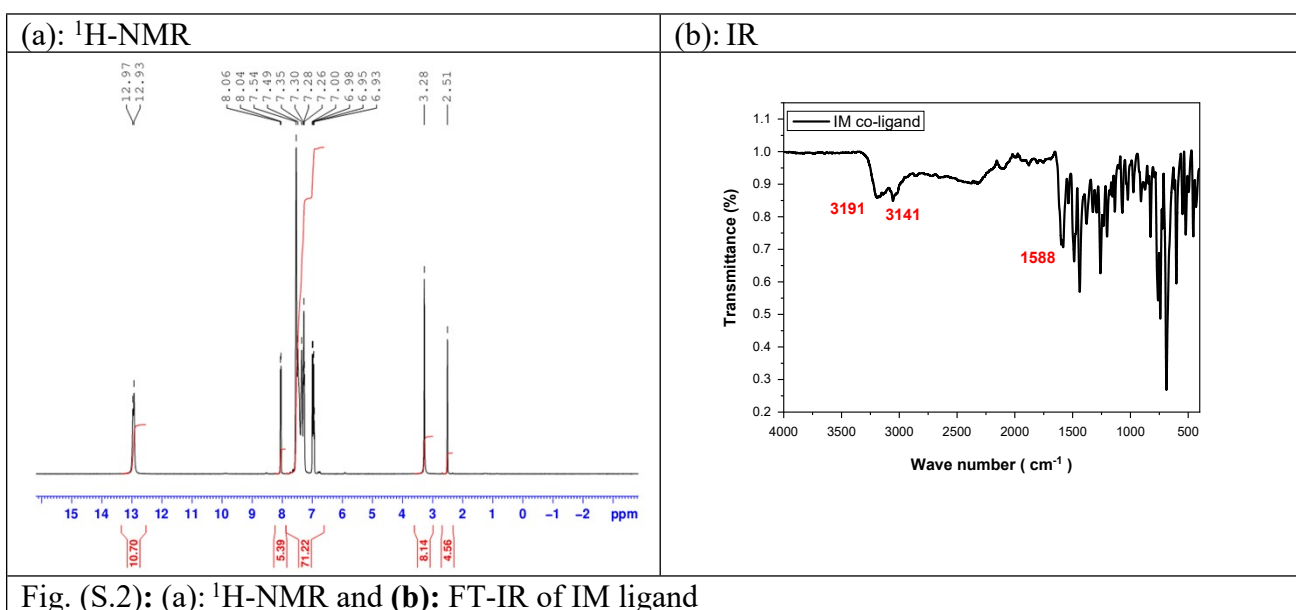
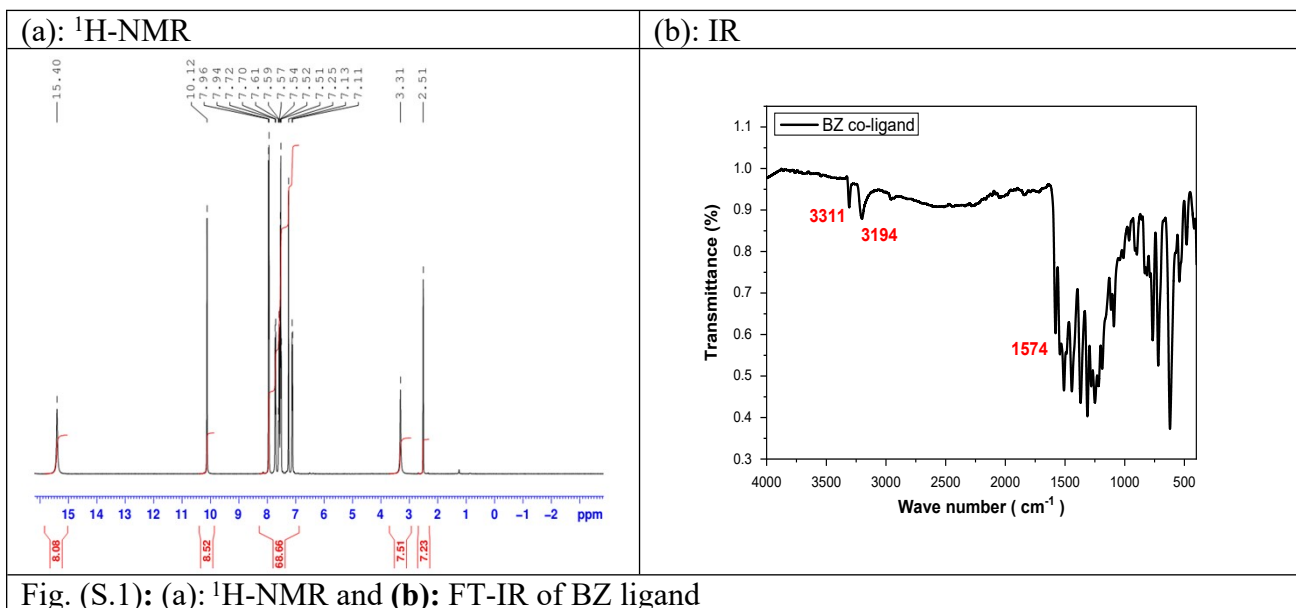
Anti-inflammatory activity

In an *in vitro* study, the anti-inflammatory effectiveness of the title products was assessed via evaluating their ability to reduce the denaturation of egg albumin (protein) [17, 18]. To conduct the experiment, a reaction mixture of five milliliters was organized via combining 0.2 milliliter of egg albumin solution (derived from fresh hen's eggs), 2 milliliters of the title components (or the standard drug Ibuprofen) at varying concentrations, and 2.8 milliliter of phosphate-buffered saline (pH 7.4). The final concentrations of the title components were adjusted to 10, 50, 100, 250, and 500 μM . As a control, a separate mixture of five milliliters was created via mixing 0.2 milliliters of egg albumin solution, two milliliter of bi-distilled water, and 2.8 milliliter of phosphate-buffered saline. Both sets of mixtures

were incubated at thirty-seven °C for thirty minutes and then heated in a water bath at seventy °C for fifteen minutes. After cooling, the absorbance of each mixture was measured at 660 nm using a UV-Vis spectrophotometer, with bi-distilled water serving as the blank. The percentage inhibition of protein denaturation was calculated using the formula:

$$\% \text{ inhibition} = \frac{A_c - A_t}{A_c} \times 100, \text{ where } A_t \text{ represents the absorbance of the test sample and } A_c$$

represents the absorbance of the control. The experiments were conducted in triplicate, with ibuprofen serving as the standard component. Additionally, the concentration of the title components or the standard drug that caused 50% inhibition (IC₅₀) was determined using <https://www.aatbio.com/tools/ic50-calculator>.



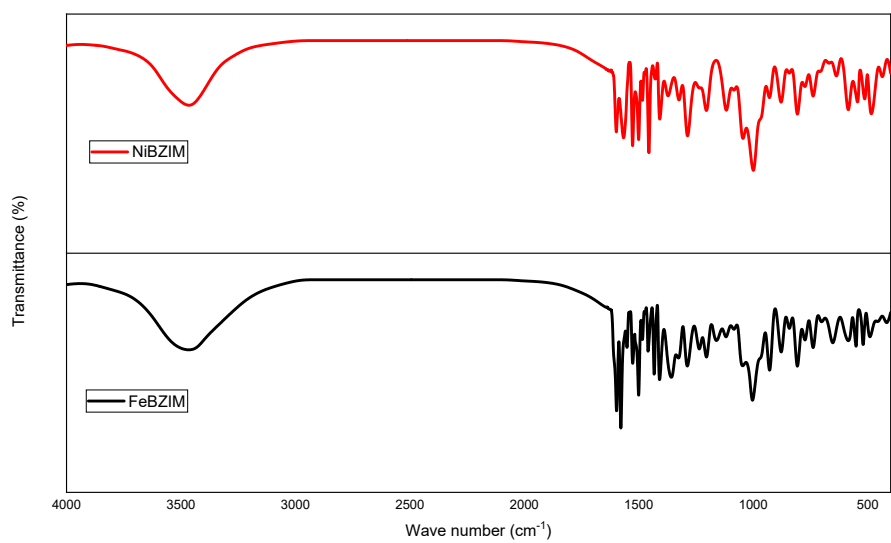


Fig. (S.3): FT-IR spectra of the FeBZIM and NiBZIM complexes

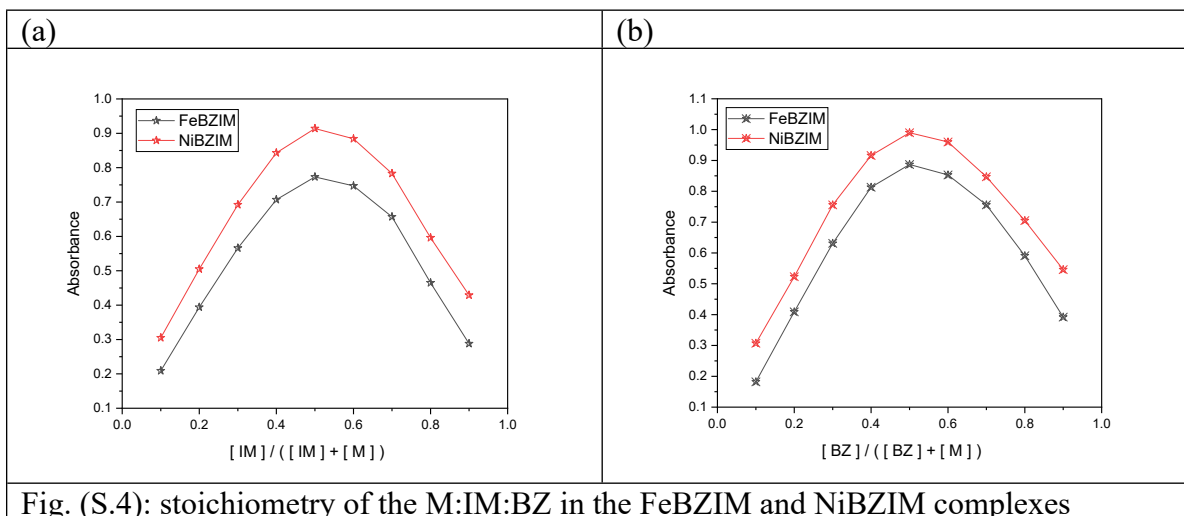


Fig. (S.4): stoichiometry of the M:IM:BZ in the FeBZIM and NiBZIM complexes

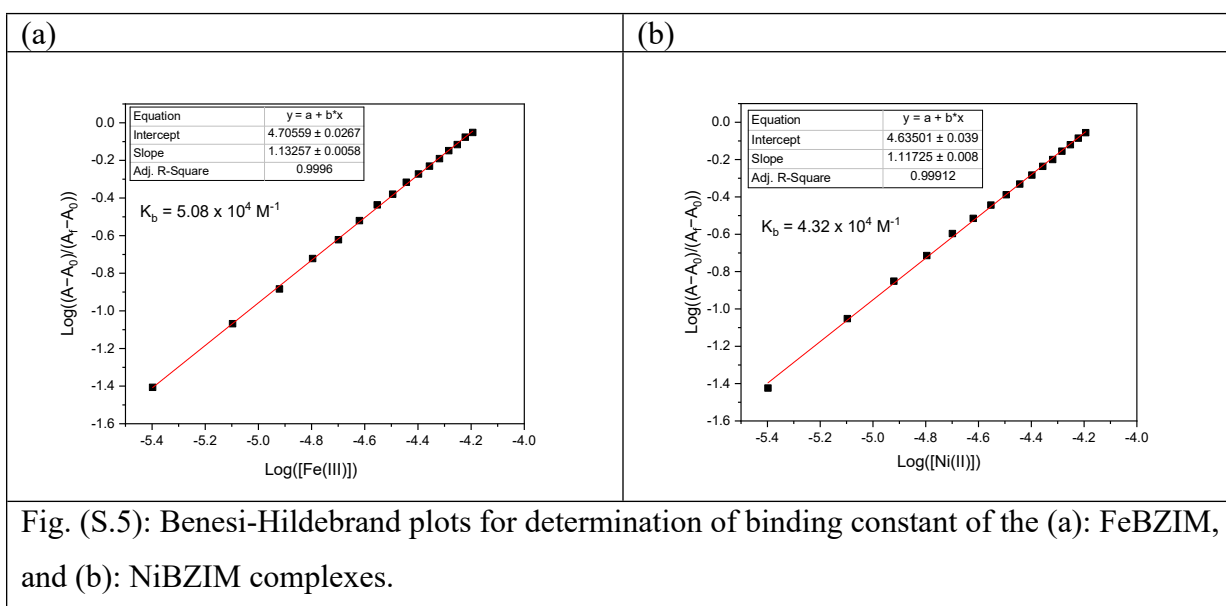


Fig. (S.5): Benesi-Hildebrand plots for determination of binding constant of the (a): FeBZIM, and (b): NiBZIM complexes.

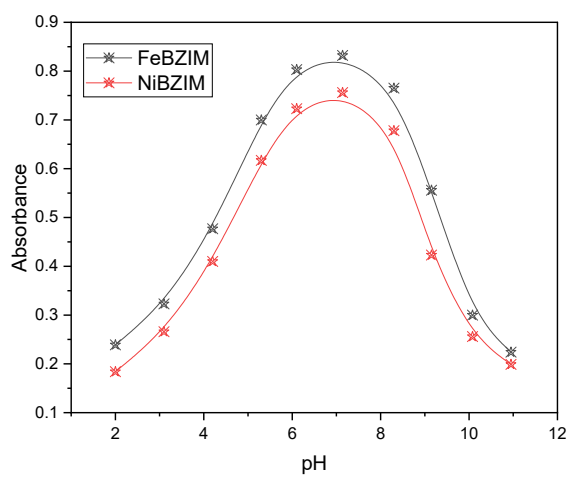


Fig. (S.6): pH stability of the prepared FeBZIM and NiBZIM complexes

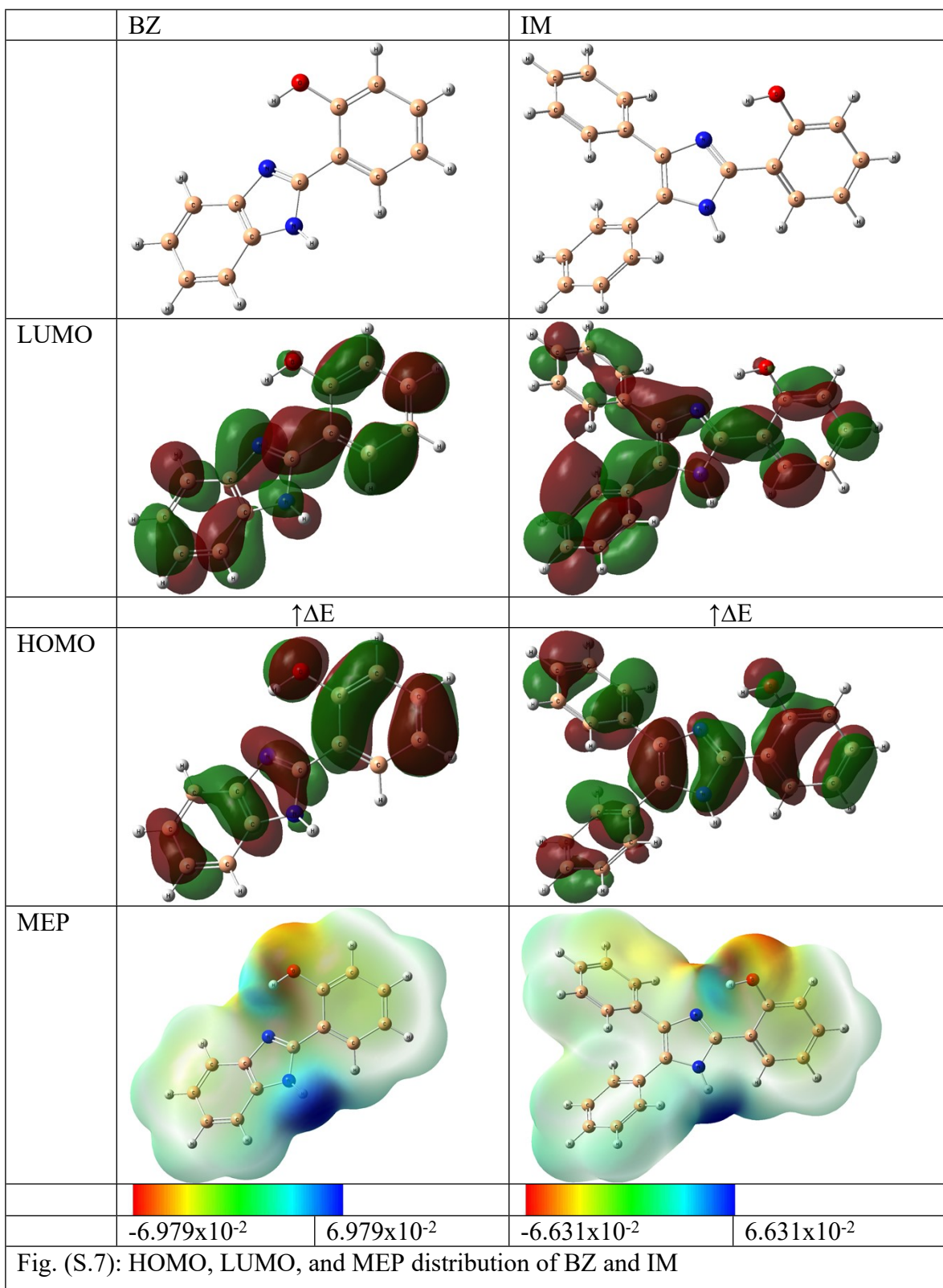


Fig. (S.7): HOMO, LUMO, and MEP distribution of BZ and IM

Table (S.1): The calculated structural parameters of the FeBZIM and NiBZIM complexes

FeBZIM		NiBZIM	
bond length (Å)		bond length (Å)	
Fe-O _{BZ}	2.01	Ni-O _{BZ}	1.95
Fe-N _{BZ}	2.07	Ni-N _{BZ}	2.01
Fe-O _{IM}	2.02	Ni-O _{IM}	1.95
Fe-N _{IM}	2.05	Ni-N _{IM}	1.99
bond angle		bond angle	
N _{IM} -Fe-O _{IM}	86.33	N _{IM} -Ni-O _{IM}	91.16
N _{IM} -Fe-O _{H2O}	89.52	N _{IM} -Ni-O _{H2O}	89.97
N _{IM} -Fe-Cl	98.09	N _{IM} -Ni-O _{H2O}	90.23
N _{IM} -Fe-O _{BZ}	83.94	N _{IM} -Ni-O _{BZ}	88.83
N _{IM} -Fe-N _{BZ}	167.79	N _{IM} -Ni-N _{BZ}	179.48
O _{BZ} -Fe-N _{BZ}	95.23	O _{BZ} -Ni-N _{BZ}	90.77
O _{BZ} -Fe-Cl	83.35	O _{BZ} -Ni-O _{H2O}	92.62
O _{BZ} -Fe-O _{H2O}	152.70	O _{BZ} -Ni-O _{H2O}	178.92
O _{BZ} -Fe-O _{IM}	101.80	O _{BZ} -Ni-O _{IM}	87.56

Table (S.2): Antibacterial activity as diameter of zone inhibition in mm				
	Diameter of zone inhibition in mm			
	Gram-positive bacteria		Gram-negative bacteria	
	<i>Bacillus Subtilis</i>	<i>Staph. Aureus</i>	<i>Escherichia coli</i>	<i>k. pneumonia</i>
BZ	11	11	12	11
IM	12	12	13	12
FeBZIM	29	29	27	27
NiBZIM	29	28	26	27
chloramphenicol	31	30	28	28

Table (S.3): Antibacterial activity as Activity index (%)				
	Activity index (%)			
	Gram-positive bacteria		Gram-negative bacteria	
	<i>Bacillus Subtilis</i>	<i>Staph. Aureus</i>	<i>Escherichia coli</i>	<i>k. pneumonia</i>
BZ	35.48	36.67	42.86	39.29
IM	38.71	40.00	46.43	42.86
FeBZIM	93.55	96.67	96.43	96.43
NiBZIM	93.55	93.33	92.86	96.43
chloramphenicol	100	100	100	100

Comp. No	Minimal Inhibitory Concentration (MIC) in μ M			
	Gram-positive bacteria		Gram-negative bacteria	
	<i>B. Subtilis</i>	<i>S. Aureu</i>	<i>E. coli</i>	<i>k. pneumonia</i>
BZ	130	120	130	120
IM	130	130	130	120
FeBZIM	90	80	80	90
NiBZIM	90	80	80	90

Comp.	Diameter of zone inhibition in mm	
	<i>Candida albicans</i>	<i>Aspergillus niger</i>
BZ	9	10
IM	11	12
FeBZIM	19	18
NiBZIM	18	18
clotrimazole	22	20

Comp.	Activity index (%)	
	<i>Candida albicans</i>	<i>Aspergillus niger</i>
BZ	40.91	50.00
IM	50.00	60.00
FeBZIM	86.36	90.00
NiBZIM	81.82	90.00
clotrimazole	100	100

Table (S.7): Antifungal activity as Minimum Inhibition Concentration (MIC, μM)		
Comp. No	Minimal Inhibitory Concentration (MIC) in μM	
	Fungi	
	<i>C. Albicans</i>	<i>Aspergillus niger</i>
BZ	140	150
IM	150	150
FeBZIM	90	100
NiBZIM	90	100

Table (S.8): Anti-inflammatory results as Mean percentage inhibition, and IC_{50} .					
Concentration (μM)	Percentage of Inhibition (%)				
	IM	BZ	FeBZIM	NiBZIM	Standard
10	2.71	4.59	7.27	6.25	19.78
50	4.56	10.66	22.06	21.26	46.86
100	9.71	23.54	38.05	37.59	76.82
250	18.21	31.19	45.62	42.51	81.18
500	22.52	41.49	55.31	54.25	82.28
IC_{50} μM	150.49	153.97	77.42	80.69	53.47

Table (S.9): Molecular docking interactions of BZ, IM ligands, and their FeBZIM, and NiBZIM, with the target 1HNJ and 5IKT proteins

1HNJ	Residues	distance	Interaction	Binding energy (kcal/mol)
BZ	ASN247	2.94	Hydrogen Bond	-7.3
	ALA246	3.60	Hydrophobic	
	MET207	5.20	Hydrophobic	
	VAL212	5.25	Hydrophobic	
	CYS112	4.95	Hydrophobic	
	LEU189	5.27	Hydrophobic	
	VAL212	5.11	Hydrophobic	
	ALA246	4.20	Hydrophobic	
	ILE156	5.29	Hydrophobic	
IM	ARG249	4.35	Electrostatic	-7.9
	ASN247	2.96	Hydrogen Bond	
	ALA246	3.65	Hydrophobic	
	ILE156	5.46	Hydrophobic	
	MET207	5.38	Hydrophobic	
	VAL212	5.02	Hydrophobic	
FeBZIM	ARG36	4.11	Electrostatic	-9.2
	ARG151	4.45	Electrostatic	
	GLY209	3.25	Hydrogen Bond	
	ASN247	3.18	Hydrogen Bond	
	PHE213	5.64	Hydrophobic	
	ARG36	5.39	Hydrophobic	
	ILE156	5.01	Hydrophobic	
	MET207	5.26	Hydrophobic	
NiBZIM	GLU211	4.98	Electrostatic	-8.9
	GLY152	2.23	Hydrogen Bond	
	ASN210	2.69	Hydrogen Bond	
	ARG249	3.66	Electrostatic	
	ARG249	3.92	Electrostatic	
	ARG36	5.37	Hydrophobic	
5IKT	Residues	distance	Interaction	Binding energy (kcal/mol)
BZ	THR206	2.11	Hydrogen Bond	-7.4
	TRP387	2.73	Hydrogen Bond	
	HIS207	4.36	Electrostatic	
	HIS386	4.36	Hydrophobic	
	HIS207	4.56	Hydrophobic	
	HIS388	4.33	Hydrophobic	
	ALA199	5.49	Hydrophobic	
	LEU391	5.35	Hydrophobic	
IM	HIS388	2.62	Hydrogen Bond	-7.1
	PHE210	2.96	Hydrogen Bond	

	HIS207	3.52	Electrostatic	
	HIS207	4.52	Electrostatic	
	HIS386	3.79	Electrostatic	
	HIS386	3.91	Hydrophobic	
	VAL291	4.65	Hydrophobic	
	LEU294	5.36	Hydrophobic	
	VAL291	4.68	Hydrophobic	
FeBZIM	HIS214	2.35	Hydrogen Bond	-9.5
	PHE210	2.02	Hydrogen Bond	
	HIS207	3.86	Electrostatic	
	HIS207	4.51	Hydrophobic	
	VAL291	4.61	Hydrophobic	
	VAL447	4.69	Hydrophobic	
	ALA450	4.96	Hydrophobic	
	VAL291	4.93	Hydrophobic	
NiBZIM	HIS207	3.09	Hydrogen Bond	-9.4
	HIS207	3.71	Electrostatic	
	HIS386	4.68	Electrostatic	
	VAL291	3.97	Hydrophobic	
	HIS386	5.02	Hydrophobic	
	VAL447	4.65	Hydrophobic	

Referances

- [1] M. Ismael, A.-M.M. Abdel-Mawgoud, M.K. Rabia, A. Abdou, Ni(II) mixed-ligand chelates based on 2-hydroxy-1-naphthaldehyde as antimicrobial agents: Synthesis, characterization, and molecular modeling, *Journal of Molecular Liquids* 330 (2021) 115611.
- [2] M. Ismael, A.-M.M. Abdel-Mawgoud, M.K. Rabia, A. Abdou, Synthesis, characterization, molecular modeling and preliminary biochemical evaluation of new copper (II) mixed-ligand complexes, *Journal of Molecular Structure* 1227 (2021) 129695.
- [3] M. Ismael, A.-M.M. Abdel-Mawgoud, M.K. Rabia, A. Abdou, Design and synthesis of three Fe(III) mixed-ligand complexes: Exploration of their biological and phenoxazinone synthase-like activities, *Inorganica Chimica Acta* 505 (2020) 119443.
- [4] J. Jayabharathi, V. Thanikachalam, K. Jayamoorthy, Physicochemical studies of chemosensor imidazole derivatives: DFT based ES IPT process, *Spectrochimica Acta Part A: Molecular and Biomolecular Spectroscopy* 89 (2012) 168-176.
- [5] J. Jayabharathi, V. Thanikachalam, N. Srinivasan, K. Jayamorthy, M.V. Perumal, An intramolecular charge transfer fluorescent probe: synthesis, structure and selective fluorescent sensing of Cu^{+2} , *Journal of fluorescence* 21 (2011) 1813-1823.
- [6] K. Ibrahim, R. Zaky, E. Gomaa, L. Yasin, Computational simulation and biological studies on 3-(2-(2-hydroxybenzoyl) hydrazono)-N-(pyridine-2-yl) butanamide complexes, *Journal of Molecular Structure* 1101 (2015) 124-138.
- [7] J. Jayabharathi, V. Thanikachalam, K. Jayamoorthy, M.V. Perumal, A physiochemical study of excited state intramolecular proton transfer process: luminescent chemosensor by spectroscopic investigation supported by ab initio calculations, *Spectrochimica Acta Part A: Molecular and Biomolecular Spectroscopy* 79(1) (2011) 6-16.

- [8] A. Gahlan, M. El-Mottaleb, N. Badawy, F. Kamale, S.H. Ali, Spectrophotometric studies on binary and ternary complexes of some metal ions with alizarin red S and cysteine, *Int. J. Adv. Res* 2(10) (2014) 570-584.
- [9] R.M. El-Khatib, L.A.-M.E. Nassr, Spectrophotometric study of some Mn (II) ternary complexes and their analytical applications, *Monatshefte für Chemie-Chemical Monthly* 140 (2009) 1139-1142.
- [10] R. Krishnan, J.S. Binkley, R. Seeger, J.A. Pople, Self-consistent molecular orbital methods. XX. A basis set for correlated wave functions, *The Journal of chemical physics* 72(1) (1980) 650-654.
- [11] P.J. Hay, W.R. Wadt, Ab initio effective core potentials for molecular calculations. Potentials for the transition metal atoms Sc to Hg, *The Journal of chemical physics* 82(1) (1985) 270-283.
- [12] W.R. Wadt, P.J. Hay, Ab initio effective core potentials for molecular calculations. Potentials for main group elements Na to Bi, *The Journal of chemical physics* 82(1) (1985) 284-298.
- [13] M. Mackeen, A. Ali, S. El-Sharkawy, M. Manap, K. Salleh, N. Lajis, K. Kawazu, Antimicrobial and cytotoxic properties of some Malaysian traditional vegetables (ulam), *Int. J. Pharm.* 35(3) (1997) 174-178.
- [14] N. Raman, A. Sakthivel, K. Rajasekaran, Synthesis and spectral characterization of antifungal sensitive Schiff base transition metal complexes, *Mycobiology* 35(3) (2007) 150-153.
- [15] A.D. Kulkarni, S.A. Patil, P.S. Badami, Electrochemical properties of some transition metal complexes: synthesis, characterization and in-vitro antimicrobial studies of Co (II), Ni (II), Cu (II), Mn (II) and Fe (III) complexes, *International Journal of Electrochemical Science* 4(5) (2009) 717-729.

- [16] I. Wiegand, K. Hilpert, R.E. Hancock, Agar and broth dilution methods to determine the minimal inhibitory concentration (MIC) of antimicrobial substances, *Nat. Protoc.* 3(2) (2008) 163-175.
- [17] A.M. El-Saghier, S.S. Enaili, A. Abdou, A.M. Hamed, A.M. Kadry, An operationally simple, one-pot, convenient synthesis, and in vitro anti-inflammatory activity of some new spirotriazolotriazine derivatives, *J. Heterocycl. Chem.* 61(1) (2024) 146-162.
- [18] H.M. Abd El-Lateef, M.M. Khalaf, A.A. Amer, A.A. Abdelhamid, A. Abdou, Antibacterial, antifungal, anti-inflammatory evaluation, molecular docking, and density functional theory exploration of 2-(1H-benzimidazol-2-yl)guanidine mixed-ligand complexes: Synthesis and characterization, *Appl. Organomet. Chem.* 38(1) (2024) e7299.